2005

# Modelling of the mechanical and mass transport properties of auxetic molecular sieves: an idealised inorganic (zeolitic) host-guest system.

Andrew Alderson
*University of Bolton*, A.Alderson@bolton.ac.uk

P. J. Davies
*University of Bolton*

K. E. Evans
*University of Exeter*

K. L. Alderson
*University of Bolton*, K.Alderson@bolton.ac.uk

J. N. Grima
*University of Malta*

# Modelling of the mechanical and mass transport properties of auxetic molecular sieves: an idealised inorganic (zeolitic) host-guest system

A. ALDERSON*, P. J. DAVIES*, K. E. EVANS†, K. L. ALDERSON* and J. N. GRIMA‡

* Centre for Materials Research and Innovation, The University of Bolton, Deane Road, Bolton BL3 5AB, UK, Tel: +44 (0)1204 903513, Fax: +44 (0)1204 370916, E-mail: A.Alderson@bolton.ac.uk

† Department of Engineering, The University of Exeter, North Park Road, Exeter EX4 4QF, UK

‡ Department of Chemistry, University of Malta, Msida MSD 06, Malta

Force field based simulations have been employed to model the structure, and mechanical and mass transport properties of the all-silica zeolite MFI (ZSM5 – $Si_{96}O_{192}$). Undeformed and deformed MFI subject to uniaxial loading in each of the 3 principal directions were investigated. The mechanical properties are predicted to include negative on-axis Poisson's ratios (auxetic behaviour) in the $x_1$-$x_3$ plane of the undeformed structure, and are strain-dependent. Transformation from positive-to-negative Poisson's ratio behaviour, and vice versa, is predicted for most on-axis Poisson's ratios at critical loading strains. Simulations of the simultaneous sorption of neopentane and benzene guest molecules onto the undeformed host MFI framework indicate a low neopentane-to-benzene loading ratio, consistent with experimental observation. The sorption of these 2 molecular species onto deformed MFI is Poisson's ratio- and strain-dependent.

Uniaxial tensile loading along a direction containing a negative on-axis Poisson's ratio leads to an increase in the loading of the larger neopentane molecules with respect to benzene, strongly correlated with the increase in volume associated with auxetic behaviour.

*Keywords:* Auxetic, negative Poisson's ratio, zeolite, mass transport, modelling

## 1. Introduction

Previously, research on materials having structural features at the micro-and macro-scales (foams and honeycombs) have demonstrated that materials having a negative Poisson's ratio, $\nu$, (i.e. they expand in width when stretched along their length) offer potential benefits in mass separation (filtration) applications [1]. These benefits arise from the increased change in the size/shape of the filter pore structure due to the high volume change characteristic of negative Poisson's ratio materials (known as *auxetic* materials [2]) under the application of an external load. Enhancements have been demonstrated for tunable filtration [3,4], entrapment and release of material within the filter pore structure [3-5], and pressure compensation as the filter becomes fouled during the filtration process [5]. Figure 1 shows schematically the release of a particulate from an auxetic honeycomb membrane (figure 1b) not easily achievable in the case of the non-auxetic honeycomb membrane (figure 1a).

[insert figure 1 here]

The experimental demonstration of the beneficial performance of auxetic honeycomb and foam sieve materials points to the potential of smaller scale auxetic materials in a variety of applications. Examples include biosensor membrane, molecular sieve, ion exchange and drug delivery applications.

At the molecular scale, a number of single-crystal materials are known to exhibit auxetic behaviour. For example, the α-cristobalite polymorph of crystalline silica is known to be auxetic [6], and 69% of the cubic elemental metals and some fcc rare gas solids are auxetic when stretched along the [110] off-axis direction [7]. A number of theoretical auxetic nanostructures have been proposed [8,9,10], including molecular analogues to the honeycomb geometry shown in figure 1 [2,11,12].

Molecular Mechanics simulations indicated auxetic behaviour in a range of idealised zeolitic cage nanostructures [13]. Zeolites are aluminosilicate framework structures containing molecular-sized cages and channels formed from an array of corner-sharing $SiO_4^{4-}$ and $AlO_4^{5-}$ tetrahedra. The presence of molecular-sized pores in the nanostructure lead to the use of zeolites in, for example, molecular sieve and ion exchange applications. Combined Molecular Mechanics and Monte Carlo simulations were used in a preliminary investigation to show that the presence of a negative Poisson's ratio enabled selective loading of neopentane and benzene guest molecules in the all-silica host zeolite MFI (ZSM5 – $Si_{96}O_{192}$) nanostructure through the application of an external stress in one specific direction [13].

In this paper we report work extending the previous preliminary mechanical property and mass transport simulations to include strain-dependent mechanical properties and an in-depth investigation into the separation behaviour due to auxetic functionality in an inorganic idealised zeolitic molecular sieve system. In a companion

paper we report simulations on mass transport properties for an idealised organic molecular network [14]

## 2. Zeolitic host-guest system

The MFI nanostructure was chosen to enable a complete and systematic study of the predicted guest molecule loading ratios for stretching along each of the 3 mutually orthogonal principal directions of the MFI framework. MFI contains two series of molecular-sized channels perpendicular to the $x_3$ direction: one running parallel to the $x_1$ direction and the other parallel to the $x_2$ direction (figure 2).

[insert figure 2 here]

Undeformed MFI has previously been predicted from Molecular Mechanics simulations to possess both negative and positive on-axis Poisson's ratios [13]. It is known that benzene molecules can be accommodated within the cavities of the undeformed MFI nanostructure, but the slightly larger neopentane molecules are excluded. The use of the Monte Carlo method in conjunction with the Molecular Mechanics method previously enabled the prediction of an increase in the loading of neopentane molecules within the MFI nanostructure when stretched in the $x_3$ direction, and was attributed in part to the opening of the molecular-sized channels due to the auxetic effect in the loading plane perpendicular to the axis of the channels [13]. MFI represents a real molecular sieve material with predicted negative and positive Poisson's

ratios and, therefore, offers the potential to identify differences in mass separation due to auxetic and non-auxetic functionality in the same molecular-level host-guest system.

## 3. Modelling methodology

The *Cerius*$^2$ Molecular Modelling software (Accelrys) was employed on a Silicon Graphics O2 workstation. The BKS force-field [15] was employed in the simulations of the structure and mechanical properties of MFI. The BKS force-field assumes interatomic interactions are ionic and was specifically developed for silicates and aluminophosphates with parameterization based on ab initio and experimental data. The modelling protocols for the structure and mechanical properties simulations were as described in detail in ref. [13].

To summarise, the starting (undeformed) structure for MFI was as provided within the *Cerius*$^2$ structure database derived from experimental data [16]. The energy expression was set up with the fixed charges supplied within the force-field. Since MFI is a purely siliceous framework a neutral unit cell was automatically attained and so charge neutralisation was not necessary. The non-bond interactions were summed using the Ewald summation procedure (used with automated cut-offs, and employing the geometric rule to compute the Van der Waals energy term coefficients) to minimise cut-off errors [17]. To ensure the minimisation achieved the correct minimum the experimentally determined unit-cell symmetry (orthorhombic space group Pnma) was applied and the potential energy of the undeformed structure was then minimised as a function of the atomic coordinates to the earliest of the default *Cerius*$^2$ standard convergence criterion (atomic RMS of 0.1Kcal/mol) or 100 minimisation steps. The

unit-cell symmetry was then reduced to P1 and the structure was minimised again to the earlier of the default *Cerius*$^2$ high convergence criterion (atomic RMS of 0.001Kcal/mol) or 5000 minimisation steps. This step was repeated three times to enable re-calculation of the non-bond list. Convergence was usually achieved within the first 5000 steps. The stiffness matrix **C** was computed from the second derivative of the energy expression, and the on-axis elastic constants were obtained directly from the compliance matrix. The Poisson's ratios ($\nu_{ij}$) were calculated from the compliance coefficients ($s_{ij}$) using

$$\nu_{ij} = -\frac{s_{ji}}{s_{ii}} \tag{1}$$

where the subscripts i and j refer to directions $x_i$ and $x_j$ parallel and perpendicular to the loading direction, respectively. The Young's moduli ($E_i$) were calculated using

$$E_i = \frac{1}{s_{ii}} \tag{2}$$

Deformed structures were modelled for uniaxial applied stresses along each of the 3 principal directions in 0.1GPa increments within the range of $-2 \leq \sigma_i \leq +2$ GPa. In the simulations of deformed structures the starting structure at each increment of applied stress was the minimised structure from the previous stress level. Checks on the elastic constants calculated using the second derivative method were performed by calculating the elastic contancts directly from the applied stresses and the resultant strains in the minimised deformed structures.

The simulation of the simultaneous sorption of benzene and neopentane molecules onto the MFI nanostructure was performed using the minimised structures for uniaxial loads applied in each of the principal directions as described above. The

Yashonath sorption force-field [18] was employed, which is designed for the sorption of small rigid molecules onto zeolites. All simulations were carried out at a sorption temperature of 300K and used the Fixed Pressure grand canonical Monte Carlo method which allows creation and destruction of sorbate molecules and varies their position and orientation. For each simulation, a free volume calculation was carried out to ensure that sorbates were not placed in areas made inaccessible due to the Van der Waals radii of the atoms in the host structure. Initial investigations were carried out to determine the required number of configurations to ensure an equilibrium had been achieved.

## 4. Results

### *4.1. Structure and Mechanical properties*

**4.1.1. Undeformed.** Table 1 contains the predicted unit-cell lengths and elastic constants (Poisson's ratios and Young's moduli) for undeformed MFI. The experimental unit-cell dimensions for MFI are also included in table 1 for comparison [16]. The predicted unit-cell lengths agree to within 2% of the experimental values.

[insert table 1 here]

There is a general lack of experimental elastic constants data for zeolite materials. However, in a previous study [13] a number of force-fields, including the BKS force-field, developed specifically to predict zeolite structure and properties were employed to predict the elastic constants for a range of zeolites. Also included in table

1, therefore, are the predicted Poisson's ratio data reported in the previous study for the BKS force-field simulations of MFI for comparison with the data reported in this paper. The current simulations on undeformed MFI yield identical Poisson's ratios to those reported previously for the BKS force-field [13]. The simulations predict negative on-axis Poisson's ratios in the $x_1$-$x_3$ plane (for uniaxial loading along both $x_1$ and $x_3$ directions), and positive on-axis Poisson's ratios in the $x_1$-$x_2$ and $x_2$-$x_3$ planes.

**4.1.2. Deformed.** Figure 3 shows the unit-cell lengths of MFI as a function of applied uniaxial stress in each of the principal directions. An abrupt change in the lattice parameters is observed for $\sigma_3 < -1.7$ GPa (figure 3c) and is indicative of a change in phase. Hence in the following, where we are concerned with the mechanical and mass transport properties of a single phase of the host MFI nanostructure, data for $\sigma_3 < -1.7$ GPa are neglected.

The variations in the unit-cell lengths with applied stress confirm the signs of the Poisson's ratios predicted from the second derivative method for the undeformed structure (i.e. zero stress). For example, in the case of an applied stress along the $x_3$ direction (i.e. $\sigma_3$, figure 3c), the unit-cell length in the $x_2$ direction ($X_2$) varies in an opposite sense to the unit-cell length ($X_3$) in the loading direction, corresponding to a positive value for $\nu_{32}$ in the range $-1.7 \leq \sigma_3 \leq 2$ GPa. On the other hand the unit-cell length in the $x_1$ direction ($X_1$) acts in the same sense as $X_3$ for $-1.7 \leq \sigma_3 < 1.1$ GPa with a corresponding negative value of $\nu_{31}$ in this stress range. For $\sigma_3 > 1.1$ GPa, $X_1$ acts in an opposite sense to $X_3$ and, therefore, indicates that $\nu_{31}$ undergoes a transition from a negative to a positive sign. These trends are confirmed in figure 4 which shows the calculated $\nu_{31}$ and $\nu_{32}$ values as a function of $\sigma_3$.

[insert figure 3 here]

[insert figure 4 here]

It is usual to present variations in mechanical properties of materials undergoing loading as a function of loading strain [20,21]. Figures 5 and 6, therefore, show the predicted Poisson's ratio and Young's modulus variations as a function of loading strain ($\varepsilon_i$) for uniaxial loading in each of the principal directions. For brevity, only those mechanical properties associated with the loading direction (and, therefore, of direct relevance to the deformation of a sieve material undergoing uniaxial loading) are presented in each case – e.g. $\nu_{12}$, $\nu_{13}$ and $E_1$ are shown as a function of $\varepsilon_1$ due to loading along the $x_1$ direction (figures 5a and 6). The mechanical properties are predicted to be strain dependent with transitions from auxetic to non-auxetic behaviour (and vice versa) occurring at critical strains in most cases. With the exception of $\nu_{32}$, all the on-axis Poisson's ratios display similar trends of becoming positive at high tensile strain and negative at increasingly compressive strain, with a minimum value at an intermediate level of compression. The value of $\nu_{32}$ remains positive throughout the strain range considered here, although it too varies with strain and approaches zero at high compressive strain (figure 5c).

[insert figure 5 here]

[insert figure 6 here]

The Young's moduli increase with increasing tensile strain, and decrease to a common value of ~23GPa at compressive strains of $\varepsilon_i \leq -2.5\%$.

### *4.2. Sorption properties*

Figure 7 shows the calculated neopentane/benzene loading ratio as a function of loading strain for uniaxial loading in each of the principal directions. The neopentane and benzene loading values for each data point are the average of the values predicted from 10 simulations. For clarity best-fit polynomial curves have been added to each data set to guide the eye.

[insert figure 7 here]

The neopentane/benzene loading ratio is predcted to be low (~0.25) for undeformed MFI, which is consistent with experimental observation that MFI adsorbs benzene but rejects the slightly larger neopentane molecules [19]. Compressive loading in any of the principal directions leads to a decrease in the loading ratio. For uniaxial tensile loading, on the other hand, the neopentane/benzene loading ratio is seen to increase considerably for loading along both the $x_1$ and $x_3$ directions, whilst the loading ratio decreases for loading along the $x_2$ direction.

## 5. Discussion

Table 1 shows that the predicted lattice parameters agree to within 2% of the experimental values for MFI. This level of agreement is typical for force-field based simulations in silicates and related materials [20,21] and demonstrates that the BKS force-field and modelling protocol employed in this work are appropriate.

Table 1 also shows the predicted mechanical properties of undeformed MFI using the BKS force-field are in good agreement with those predicted previously [13] with this force-field. The negative sign of $\nu_{13}$ and $\nu_{31}$ was also previously reproduced by other force-fields (CVFF [22] and Universal [23,24]), giving some confidence that these Poisson's ratios will be negative in reality. However, lower magnitudes were predicted by these other force-fields and another force-field considered suitable for materials of this type (Burchart [25]) predicted low positive values for these Poisson's ratios. Clearly, there is a need for accurate experimental measurement of the single-crystal elastic constants for zeolite MFI to verify the accuracy of force-field based simulations for mechanical properties predictions in this material.

In this work we have extended the previous study of the mechanical properties of undeformed MFI to consider the mechanical properties of deformed MFI subjected to uniaxial loading in each of the 3 principal directions. Strains of the order of a few percent were applied and so are unlikely to be realised in practice for zeolites, which would be expected to fracture before such relatively high strain levels were reached. Nevertheless, this theoretical system enables a good model with which to investigate strain-dependent mechanical properties of a novel molecular sieve predicted to possess both positive and negative Poisson's ratios. The variation of Poisson's ratio (and hence the response of the lateral dimensions with respect to loading direction) have been taken

into account when performing a critical analysis of the mass transport simulations for MFI.

The mechanical properties are predicted to be strain-dependent and non-linear (Figs. 5 and 6), including transformation from auxetic to non-auxetic behaviour at a critical loading strain. Strain-dependent, non-linear mechancial properties (including auxetic to non-auxetic transitions in some cases) have been predicted and/or experimentally measured in other auxetic materials, including polymeric and metallic foams [26,27], microporous polymers [28,29], and at the molecular level in the α-cristobalite and α-quartz polymorphs of crystalline silica [20].

The predicted presence of negative values of $\nu_{13}$ and $\nu_{31}$ for undeformed MFI indicates that the volume will increase due to the change in the lattice parameters ($X_1$ and $X_3$) along the $x_1$ and $x_3$ directions, respectively, for tensile loading in either of these directions. For tensile loading along the $x_2$ direction, however, the predicted positive values of $\nu_{23}$ and $\nu_{21}$ will lead to decreasing values of $X_3$ and $X_1$, respectively, to counteract the volume increase due to the increase in the $X_2$ lattice parameter. This is confirmed in figure 8 which shows the fractional volume (deformed volume V divided by the undeformed volume $V_0$, calculated from the lattice parameter data in figure 3) as a function of loading strain. The volume decreases for compressive loading in each of the principal directions. For tensile loading, the volume increases for loading along each of the $x_1$ and $x_3$ directions (which have negative on-axis Poisson's ratios associated with them), whereas the volume remains approximately constant (in fact decreases slightly due to the relatively large positive $\nu_{21}$ and $\nu_{23}$ values) for loading along $x_2$.

[insert figure 8 here]

The sorption simulations on zeolite MFI indicate a clear Poisson's ratio-related effect on the mass transport properties (within the same host-guest system) for a molecular sieve undergoing external uniaxial loading (figure 7). Uniaxial tensile loading along the $x_1$ and $x_3$ directions leads to an increase in the neopentane/benzene loading ratio. This is consistent with the increase in volume associated with the negative Poisson's ratios for tensile loading along $x_1$ and $x_3$ (figure 8), which will lead to a concomitant increase in the free volume accessible to the larger neopentane molecules. On the other hand, uniaxial tensile loading along the $x_2$ direction leads to a slight reduction in the neopentane/benzene loading ratio, consistent with the slight decrease in volume due to the (large) positive Poisson's ratios for tensile loading along $x_2$. Compressive loading in any of the principal directions leads to a decrease in the loading ratio, which is consistent with the decrease in volume of the host nanostructure.

The correlation of the sorption data with the Poisson's ratio-determined volume change for uniaxial loading in all 3 principal directions is shown in figure 9. The data for all 3 loading direction scenarios are seen to follow a universal curve for this host-guest system. The increased neopentane/benzene loading ratios for $V/V_0 > 1$ can only be achieved for tensile loading along an axis with a negative on-axis Poisson's ratio associated with it, indicating the potential for auxetic molecular sieves in the control of the relative loading of multiple molecular species within a host nanostructure.

[insert figure 9 here]

The Young's moduli variations with loading strain indicate a convergence of values at ~ 23 GPa for compressive loading strains ≤ -0.025 and increasing values for strains > 0.01 (figure 6). An explanation for the convergence to a common low Young's modulus value under uniaxial compression will require a detailed examination of the structure of the deformed MFI framework under the different loading conditions, and possibly application of analytical models which consider the possible deformation modes of the 3D sub-units of the framework (e.g. $SiO_4$ tetrahedra) [21,30] and their 2D projections in specific crystal planes (e.g. squares and triangles) [13]. The implication of the increasing Young's moduli with increasing tensile strain in this tunable molecular sieve is that the benefits due to auxetic functionality will require a higher level of applied stress to achieve the required deformation.

Finally, the indication of a stress-induced phase transition at $\sigma_3$ ~ -1.8 GPa (figure 3c) has been neglected from consideration in this paper in which we have concentrated on the strain-dependent mechanical and mass transport properties of a single-phase molecular sieve. However, we note that a phase change may also be potentially useful in the entrapment and release of molecules. We also note here that stress-induced phase transformations have previously been predicted in related materials [21] and that phase transitions can be acompanied by interesting changes in the mechanical properties (including auxetic-to-nonauxetic transitions and vice versa) [21,31].

## 6. Summary

In summary, force-field based simulations have been performed to predict auxetic (negative Poisson's ratio) properties in the all silica zeolite MFI. The mechanical properties are predicted to be strain-dependent and include the transformation of negative-to-positive Poisson's ratios (and vice versa) at critical loading strains. Monte Carlo simulations of the simultaneous sorption of benzene and (slightly larger) neopentane molecules onto the MFI nanostructure indicate the sorption is strain dependent and also Poisson's ratio dependent. The neopentane-to-benzene loading ratio is low for undeformed MFI, consistent with experimental observation. Loading along a direction with only positive on-axis Poisson's ratios associated with it is unable to increase this loading ratio significantly. However, tensile loading along a direction demonstrating a negative on-axis Poisson's ratio leads to an increase in volume which enables increased loading of the neopentane molecules with respect to benzene. Compressive uniaxial loading in all directions leads to a decrease in volume and a lowering of the neopentane-to-benzene ratio.

| | This work (BKS) | Experimental [16] | Previous modelling [13] | | | |
|---|---|---|---|---|---|---|
| | | | BKS | Bur | CVFF | Uni |
| $X_1$ (Å) | 20.238 | 20.022 | | | | |
| $X_2$ (Å) | 20.318 | 19.899 | | | | |
| $X_3$ (Å) | 13.641 | 13.383 | | | | |
| $\nu_{12}$ | +0.23 | | | | | |
| $\nu_{13}$ | -0.14 | | -0.14 | +0.08 | -0.02 | -0.08 |
| $\nu_{21}$ | +0.52 | | | | | |
| $\nu_{23}$ | +0.35 | | +0.35 | +0.46 | +0.30 | +0.54 |
| $\nu_{31}$ | -0.35 | | -0.35 | +0.08 | -0.02 | -0.06 |
| $\nu_{32}$ | +0.39 | | +0.38 | +0.34 | +0.27 | +0.38 |
| $E_1$ (GPa) | 26.6 | | | | | |
| $E_2$ (GPa) | 59.7 | | | | | |
| $E_3$ (GPa) | 66.5 | | | | | |

Table 1. Calculated unit-cell lengths and elastic contants (Poisson's ratios and Young's moduli) from BKS force-field simulations on zeolite MFI (ZSM5 – $Si_{96}O_{192}$). Experimental unit-cell lengths [16] and previous molecular modelling predictions [13] for selected Poisson's ratios are included for comparison (BKS = BKS force-field [15]; Bur = Burchart force-field [25]; CVFF = consistent valence force-field [22]; Uni = Universal force-field [23,24]).

**Figure Captions**

Figure 1: Schematic of particulate de-fouling capabilities of auxetic and non-auxetic honeycomb membrane filters. Both honeycombs deform by 'hinging' of the cell walls in response to an applied load.

Figure 2: $x_1$-$x_3$ and $x_2$-$x_3$ projections of 2x2x2 unit-cell MFI framework, using $SiO_4$ tetrahedra representation.

Figure 3: Lattice parameters ($X_1$, $X_2$ and $X_3$) as a function of uniaxial applied stress along (a) the $x_1$ direction, (b) the $x_2$ direction, and (c) the $x_3$ direction.

Figure 4: Poisson's ratios ($\nu_{31}$ and $\nu_{32}$) versus stress applied along the $x_3$ direction ($\sigma_3$).

Figure 5: Poisson's ratios ($\nu_{ij}$) in the loading direction versus loading strain ($\varepsilon_i$) for uniaxial loads applied along (a) the $x_1$ direction, (b) the $x_2$ direction, and (c) the $x_3$ direction.

Figure 6: Young's Modulus ($E_i$) in the loading direction versus loading strain ($\varepsilon_i$) for uniaxial loads applied along the $x_1$ direction ($E_1$), the $x_2$ direction ($E_2$), and the $x_3$ direction ($E_3$).

Figure 7: Neopentane-to-benzene loading ratios versus loading strain for uniaxial loads applied along the $x_1$ direction ($\sigma_1$), the $x_2$ direction ($\sigma_2$), and the $x_3$ direction ($\sigma_3$).

Polynomial fitted curves are also shown to guide the eye (short dash = $\sigma_1$, long dash = $\sigma_2$, solid = $\sigma_3$).

Figure 8: Fractional volume ($V/V_0$) versus loading strain for uniaxial loads applied along the $x_1$ direction ($\sigma_1$), the $x_2$ direction ($\sigma_2$), and the $x_3$ direction ($\sigma_3$).

Figure 9: Neopentane-to-benzene loading ratios versus fractional volume for uniaxial loads applied along the $x_1$ direction ($\sigma_1$), the $x_2$ direction ($\sigma_2$), and the $x_3$ direction ($\sigma_3$). A polynomial fitted curve to all the data points is also shown to guide the eye.

Figure 1

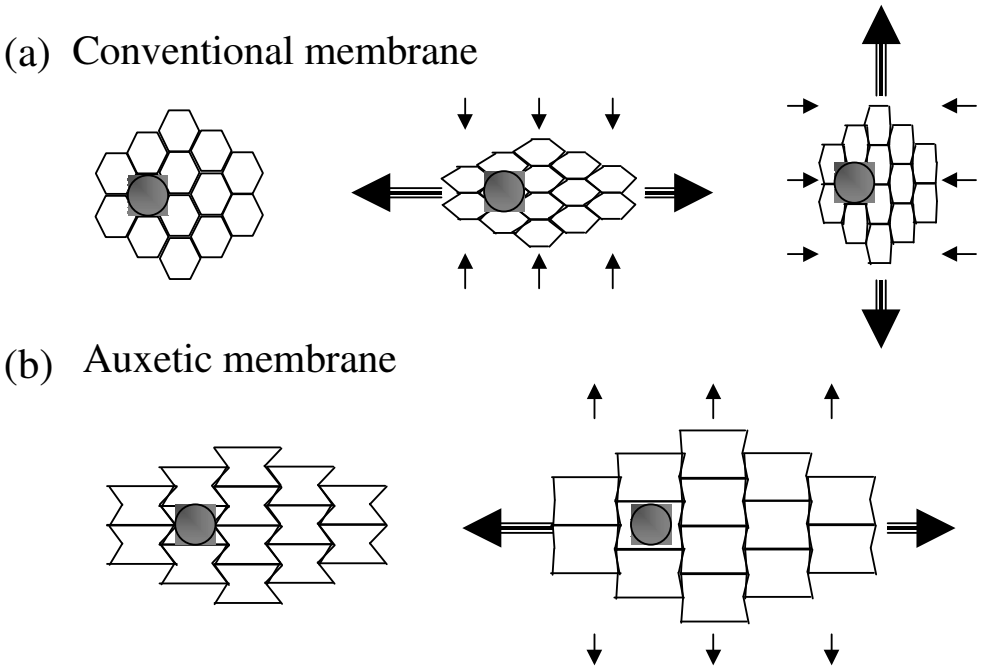

Figure 2

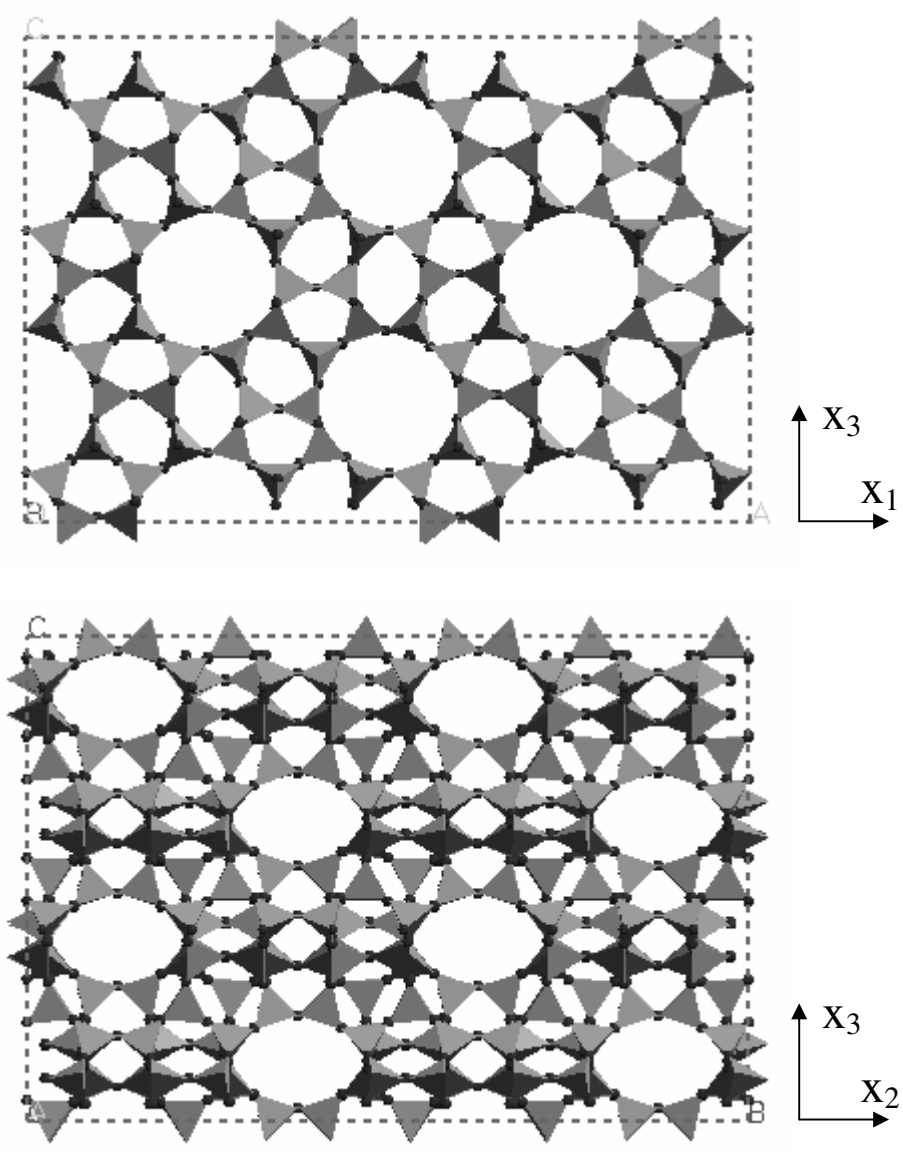

Figure 3

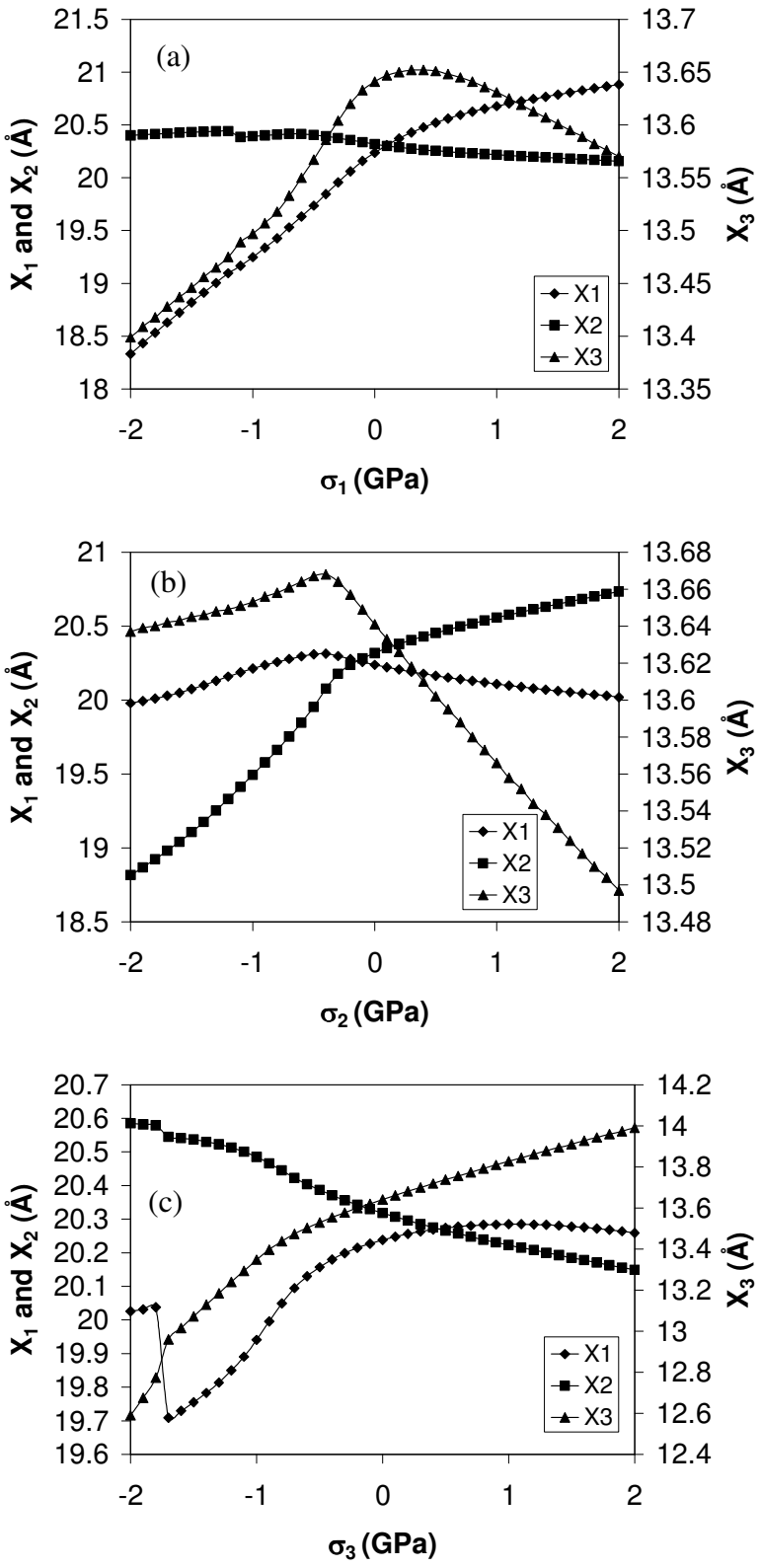
(a)
X1 and X2 (Å)
X3 (Å)
σ1 (GPa)
X1
X2
X3
(b)
X1 and X2 (Å)
X3 (Å)
σ2 (GPa)
X1
X2
X3
(c)
X1 and X2 (Å)
X3 (Å)
σ3 (GPa)
X1
X2
X3

Figure 4

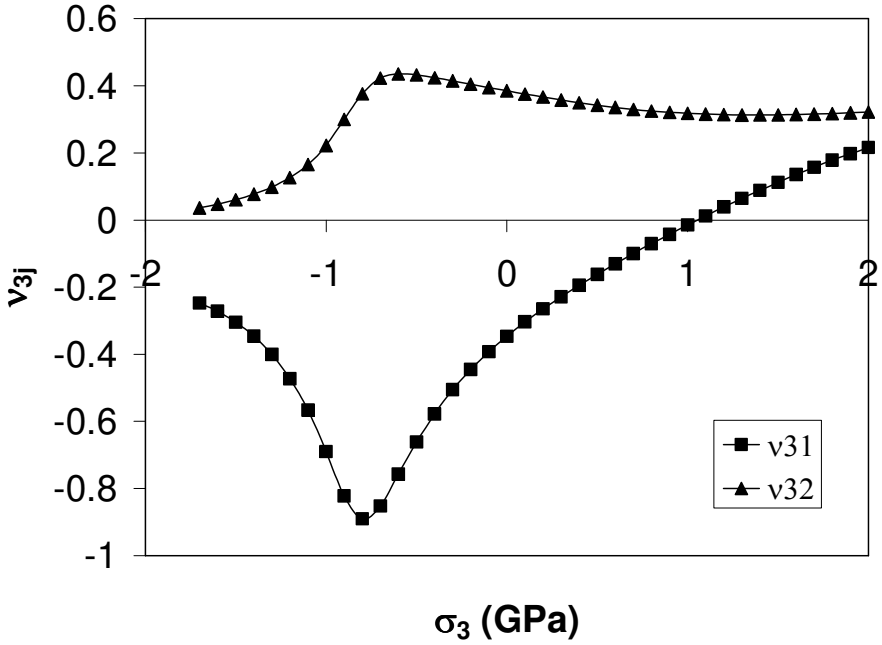

Figure 5

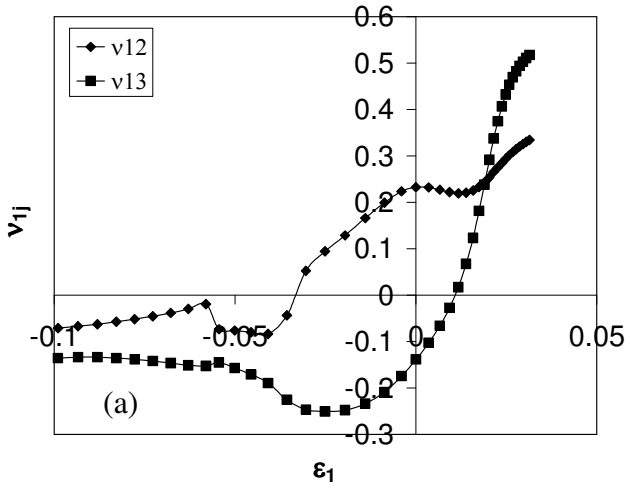
ν12
ν13
0.6
0.5
0.4
0.3
0.2
0.1
0
-0.1
-0.2
-0.3
-0.1
-0.05
0
0.05
ν1j
(a)
ε1

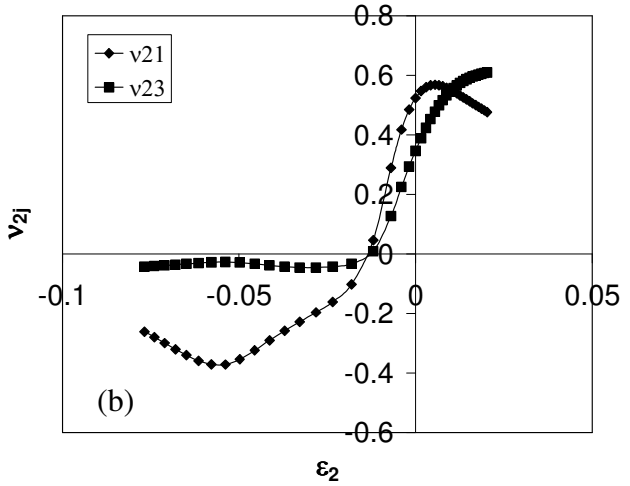
ν21
ν23
0.8
0.6
0.4
0.2
0
-0.2
-0.4
-0.6
-0.1
-0.05
0
0.05
ν2j
(b)
ε2

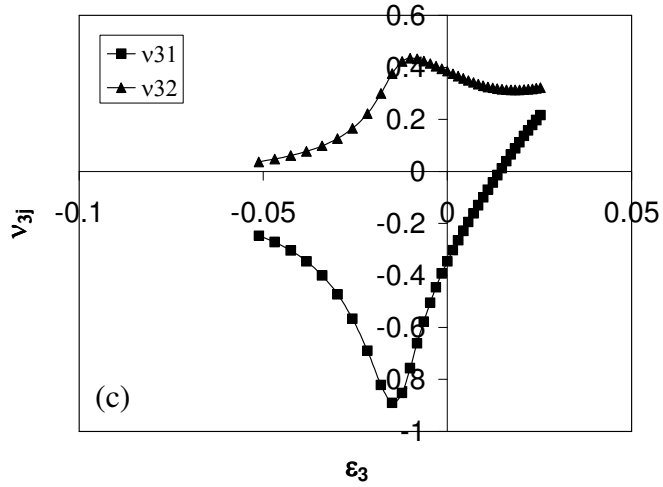
ν31
ν32
0.6
0.4
0.2
0
-0.2
-0.4
-0.6
-0.8
-1
-0.1
-0.05
0
0.05
ν3j
(c)
ε3

Figure 6

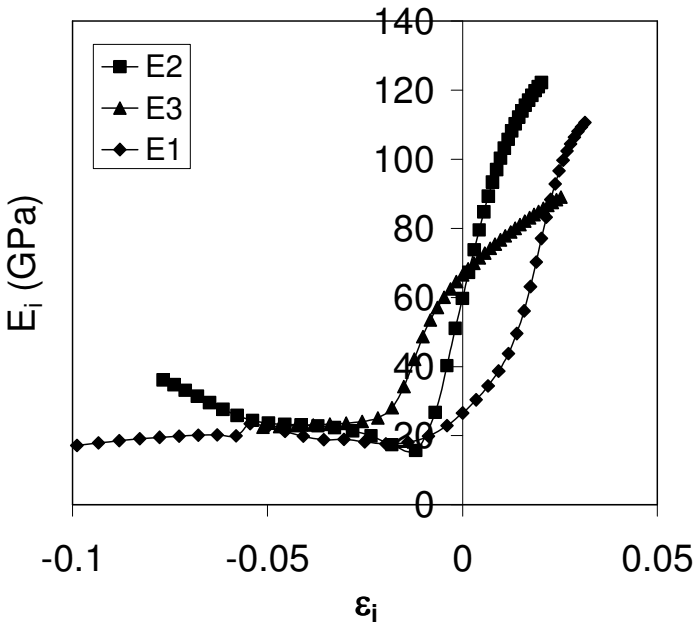

Figure 7

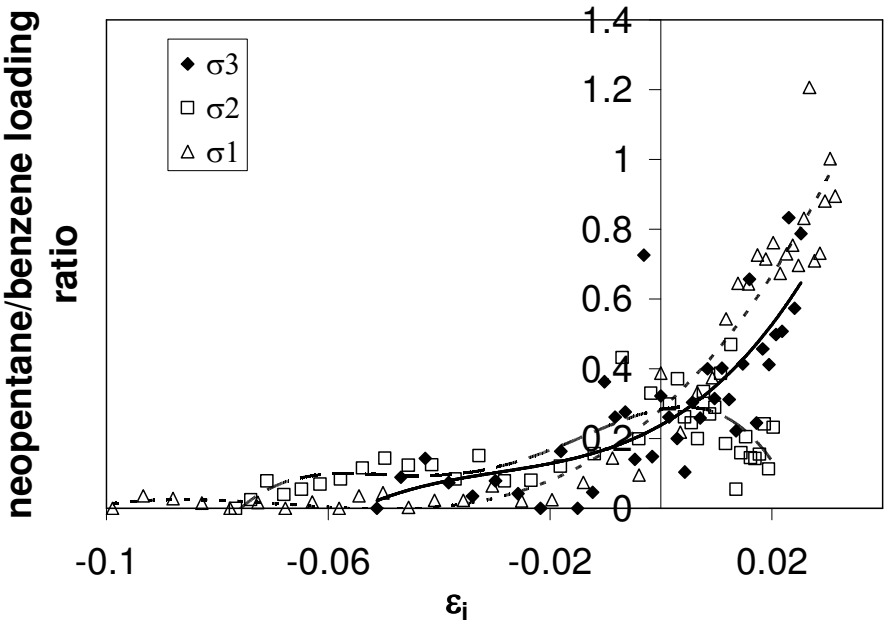
neopentane/benzene loading ratio
σ3
σ2
σ1
1.4
1.2
1
0.8
0.6
0.4
0.2
0
-0.1
-0.06
-0.02
0.02
εi

Figure 8

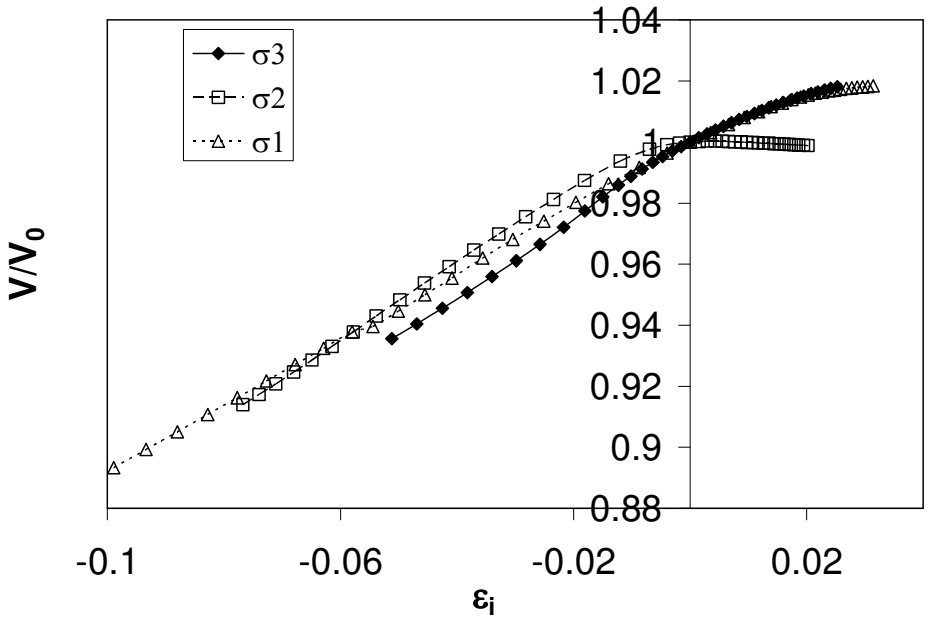

Figure 9

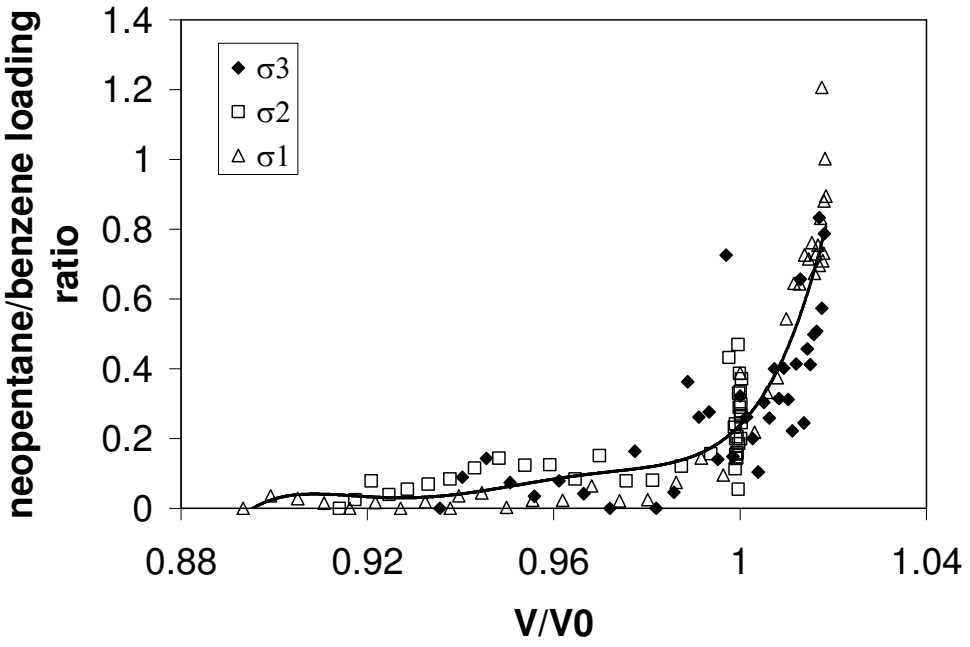
neopentane/benzene loading ratio
1.4
1.2
1
0.8
0.6
0.4
0.2
0
σ3
σ2
σ1
0.88
0.92
0.96
1
1.04
V/V0

**Acknowledgements**

The authors are grateful to the UK's Engineering and Physical Sciences Research Council for funding this work.

**References**

[1] A. Alderson, K.E. Evans, J. Rasburn. *PCT Patent*, No. WO 99/22838, Published May 1999.

[2] K.E Evans, M.M. Nkansah, I.J. Hutchinson, S.C. Rogers. Molecular network design. *Nature,* **353**, 124 (1991).

[3] A. Alderson, J. Rasburn, S. Ameer-Beg, P.G. Mullarkey, W. Perrie, K.E. Evans. An auxetic filter: a tuneable filter displaying enhanced size selectivity or de-fouling properties. *Ind. Eng. Chem. Res.*, **39**, 654 (2000).

[4] J. Rasburn, A. Alderson, S. Ameer-Beg, P.G. Mullarkey, W. Perrie, K.E. Evans. Auxetic structures for variable permeability systems. *AIChE Journal*, **47(11)**, 2623 (2001).

[5] A. Alderson, J. Rasburn, K.E. Evans, J.N. Grima. Auxetic polymeric filters display enhanced de-fouling and pressure-compensation properties. *Membrane Technology*, **137**, 6 (2001).

[6] Y. Yeganeh-Haeri, D.J. Weidner, J.B. Parise. Elasticity of α-cristobalite: a silicon dioxide with a negative Poisson's ratio. *Science*, **257**, 650 (1992).

[7] R.H. Baughman, J.M. Shacklette, A.A. Zakhidov, S. Stafstrom. Negative Poisson's ratios as a common feature of cubic metals. *Nature*, **392**, 362 (1998).

[8] K.W. Wojciechowski. Constant thermodynamic tension Monte Carlo studies of elastic properties of a two-dimensional system of hard cyclic hexamers. *Molecular Physics*, **61**, 1247 (1987).

[9] R.H. Baughman, D.S. Galvao. Crystalline networks with unusual predicted mechanical and thermal properties. *Nature*, **365**, 735 (1993).

[10] C. He, P. Liu, A.C. Griffin. Toward negative Poisson ratio polymers through molecular design. *Macromolecules*, **31**, 3145 (1998).

[11] K.E. Evans, A. Alderson, F.R. Christian. Auxetic two-dimensional polymer networks: an example of tailoring geometry for specific mechanical properties. *J. Chem. Soc. Far. Trans.*, **91**, 2671 (1995).

[12] F.R. Attenborough, K.E. Evans, A. Alderson, B.R. Eggen, M.I. Heggie. Tailoring the elastic constants of two and three dimensional molecular networks. In Proceedings of the 10th International Conference on Deformation, Yield and Fracture of Polymers, Cambridge, UK, 1997. *Inst. Matls.* 27 (1997).

[13] J.N. Grima, R. Jackson, A. Alderson, K.E. Evans. Do zeolites have negative Poisson's ratios? *Adv. Mater.*, **12**(24), 1912 (2000).

[14] A. Alderson, P.J. Davies, M.R. Williams, K.E. Evans, K.L. Alderson, J.N. Grima. Modelling of the mechanical and mass transport properties of auxetic molecular sieves: an idealised organic (polymeric honeycomb) host-guest system. *Molecular Simulation*, (2005), submitted.

[15] B.W.H. van Beest, G.J. Kramer, R.A. van Santen. Force fields for silicas and aluminophosphates based on *ab initio* calculations. Phys. Rev. Lett., **64**, 1955 (1990).

[16] G.T. Kokotailo, S.L. Lawton, D.H. Olson, W.M. Meier. Structure of synthetic zeolite ZSM-5. *Nature*, **272**, 437 (1978).

[17] N. Karasawa, W.A. Goddard. Acceleration of convergence for lattice sums. *J. Phys. Chem.*, **93**, 7320 (1989).

[18] S. Yashonath, J.M. Thomas, A.K. Nowak, A.K. Cheetham. The siting, energetics and mobility of saturated hydrocarbons inside zeolitic cages: methane in zeolite Y. *Nature*, **331**, 601 (1988).

[19] E.M. Flanigen, J.M. Bennett, R.W. Grose, J.P. Cohen, R.L. Patton, R.M. Kirchner, J.V. Smith. Silicalite, a new hydrophobic crystalline silica molecular sieve. *Nature*, **271**, 512 (1978).

[20] N.R. Keskar, J.R. Chelikowsky. Structural properties of nine silica polymorphs. Phys. Rev. B, **46**, 1 (1992).

[21] A. Alderson, K. L. Alderson, K. E. Evans, J. N. Grima, M. R. Williams, P. J. Davies. Modelling the deformation mechanisms, structure-property relationships and applications of auxetic nanomaterials. *Phys. Stat. Sol. B* **242(3),** 499 (2005).

[22] *Force-Field Based Simulations Cerius2 User Guide* (MSI Inc., San Diego, USA, **1996**).

[23] A.K. Rappe, W.A. Goddard. Charge equilibration for molecular dynamics simulations. *J. Phys. Chem.*, **95**, 3358 (1991).

[24] A.K. Rappe, C.J. Casewit, K.S. Colwell, W.A. Goddard III, W.M. Skiff. UFF, a full periodic table force field for molecular mechanics and molecular dynamics simulations. *J. Am. Chem. Soc.*, **114**, 10046 (1992).

[25] E. Vos Burchart. Studies on Zeolites: Molecular Mechanics, Framework Stability and Crystal Growth. PhD thesis, Delft University of Technology, The Netherlands (1992).

[26] R.S. Lakes. Foam structures with a negative Poisson's ratio. *Science*, **235**, 1038 (1987).

[27] J.B. Choi, R.S. Lakes. Nonlinear properties of metallic cellular materials with a negative Poisson ratio. *J. Mater. Sci.*, **27**, 5375 (1992).

[28] B.D. Caddock, K.E. Evans. Microporous materials with negative Poisson's ratios. I. Microstructure and mechanical properties. *J. Phys. D: Appl. Phys*., **22**, 1877 (1989).

[29] K.L. Alderson, A. Alderson, K.E. Evans. The interpretation of the strain-dependent Poisson's ratio in auxetic polyethylene. *J. Strain Analysis*, **32**, 201 (1997).

[30] A. Alderson, K.E. Evans**.** Molecular Origin of Auxetic Behaviour in Tetrahedral Framework Silicates. *Phys. Rev. Lett.* **89(22)**, 225503-1 (2002).

[31] S. Hirotsu. Softening of bulk modulus and negative Poisson's ratio near the volume phase transition of polymer gels. *J Chem Phys.* **94**, 3949 (1991).